applied sciences

MDPI

Article

Prediction of Particle Settling Velocity in Newtonian and Power-Law Fluids Using Artificial Neural Network Model

Weiping Lv [1], Zhengming Xu [2,*], Xia Jia [1], Shiming Duan [3], Jiawei Liu [1] and Xianzhi Song [3]

[1] Jianghan Machinery Research Institute Limited Company of CNPC, Wuhan 430024, China; lvwp@cnpc.com.cn (W.L.); jiaxdr@cnpc.com.cn (X.J.)
[2] School of Energy Resources, China University of Geosciences, Beijing 100083, China
[3] School of Petroleum Engineering, China University of Petroleum, Beijing 102249, China
* Correspondence: xuzm@cugb.edu.cn; Tel.: +86-18810982251

Abstract: In petroleum engineering, accurately predicting particle settling velocity during various stages of a well's life cycle is vital. This study focuses on settling velocities of both spherical and non-spherical particles in Newtonian and non-Newtonian fluids. Utilizing a dataset of 931 experimental observations, an artificial neural network (ANN) model with a 7-42-1 architecture is developed (one input layer, one hidden layer with 42 neurons, and one output layer). This model effectively incorporates particle settling orientation and the inclusion of the settling area ratio, enhancing its predictive accuracy. Achieving an average absolute relative error (AARE) of 8.51%, the ANN model surpasses traditional empirical correlations for settling velocities in both Newtonian and power-law fluids. Key influencing factors, such as the consistency index and particle equivalent diameter, were identified. This approach in ANN model construction and data analysis represents a significant advancement in understanding particle dynamics.

Keywords: settling velocity; artificial neural network; Newtonian fluid; power-law fluid; spherical particle; non-spherical particle

Citation: Lv, W.; Xu, Z.; Jia, X.; Duan, S.; Liu, J.; Song, X. Prediction of Particle Settling Velocity in Newtonian and Power-Law Fluids Using Artificial Neural Network Model. *Appl. Sci.* **2024**, *14*, 826. https://doi.org/10.3390/app14020826

Academic Editor: Francesca Scargiali

Received: 23 November 2023
Revised: 16 January 2024
Accepted: 17 January 2024
Published: 18 January 2024

1. Introduction

Particle transport plays a crucial role in various stages of a well's life cycle in petroleum engineering [1]. Examples include cuttings transport during drilling [2,3], sand production during oil production [4,5], and proppant transport during fracturing stimulation [6,7]. The accurate prediction of particle settling velocity is critical to describe particle transport characteristics in the wellbore. For instance, particles cannot be removed from the wellbore if the fluid velocity is smaller than the particle settling velocity in a vertical well [8,9]. Similarly, in horizontal sections of the wellbore or fractures, the transport distance of cuttings or proppants is primarily determined by the particle settling velocity [10,11]. In the study of particle dynamics, particularly in fluid mediums, two key concepts are paramount: free and hindered settling [12,13]. Free settling occurs when particles descend through a fluid independently, unaffected by the presence of other particles. This process is typically observed in dilute suspensions where particle interactions are minimal. Conversely, hindered settling describes the scenario where particle concentration is high enough that interactions between particles significantly affect their settling behavior. Hindered settling is often characterized by reduced settling velocities compared to free settling due to mutual interference among particles. Understanding these two settling regimes is crucial as they provide fundamental insights into the behavior of particles in various fluid environments, including both Newtonian and non-Newtonian fluids.

The settling characteristics of spherical particles in Newtonian fluids are well understood, as only one parameter, diameter, is sufficient to describe the particle shape [14]. However, non-spherical particles and non-Newtonian fluids are more common in petroleum

engineering, making it difficult to describe settling behaviors [15,16]. Non-spherical particles are affected not only by their shape but also their settling orientation, making their characteristics harder to describe. Thus, additional parameters are needed to describe non-spherical particle shapes, in addition to the equivalent diameter of the sphere with the same volume. Parameters for evaluating particle shape, such as the Corey shape factor [17] and circularity [18], are sometimes used. The Corey shape factor refers to the combination of lengths of the longest, the intermediate, and the shortest mutually perpendicular axes, commonly used in sedimentology to describe particle irregularity. Circularity measures how closely a particle's shape approximates a circle, with higher values indicating shapes more akin to perfect circles. However, sphericity is emphasized as the key metric. Defined as the ratio of the surface area of a sphere (with the same volume as the particle) to the surface area of the particle, sphericity accurately reflects shape deviation [19]. A sphericity value of 1 indicates a perfect sphere, with lower values signifying greater deviations. This metric is crucial in the settling velocity correlation to incorporate the impact of particle shape. Merely using sphericity is insufficient to describe the shape of non-spherical particles, as two particles with the same sphericity can have entirely different shapes and settling characteristics. The orientation of a particle also affects its drag coefficient and settling velocity. The drag force increases with the larger projected area of the particles perpendicular to the flow direction, which in turn affects the final settling velocity. However, sphericity alone cannot account for the effect of settling direction. Settling orientation also affects the particle settling process. And this phenomenon has been observed by many researchers [18,20–28].

To account for the settling orientation effect, researchers have utilized various methods. For example, Hölzer and Sommerfeld [22] incorporated two additional sphericities in the crosswise and lengthwise directions to describe the settling orientation effect, but their study only focused on predicting the drag coefficient and did not investigate the settling velocity. Another approach is to use the settling area ratio (S), as utilized by Song et al. [29]. However, their model is only applicable to Newtonian fluids. Some scholars have employed numerical simulation methods to study the influence of settling orientation [25]. However, such methods are computationally expensive. The traditional methods for predicting settling characteristics have limitations, as they only consider either spherical or non-spherical particles in either Newtonian or non-Newtonian fluids. In petroleum engineering, where both types of fluids are common, the lack of formulas capable of predicting settling velocity for both particle shapes in both types of fluids is a significant drawback of the traditional approach. Furthermore, using different correlations for different fluids and particle shapes adds complexity to the process. For instance, non-Newtonian fluids require different correlations than Newtonian fluids.

Artificial intelligence (AI) technology has gained significant attention in the petroleum engineering industry in recent years. Table 1 summarizes several studies that use AI technology to predict the drag coefficient and settling velocity of particles. Rooki et al. [30] developed an artificial neural network (ANN) to predict the terminal velocity of solid spheres, taking into account the properties of the sphere and the surrounding liquid. The ANN was trained on 88 sets of both Newtonian and non-Newtonian fluids data from published sources, accurately predicting terminal velocity of solid spheres falling through a wide range of power-law values (1.0 to 0.06). Goldstein and Coco [31] presented a novel machine learning approach, specifically using genetic programming, to predict noncohesive particle settling velocity. It utilizes a database of 985 published experimental measurements and outperforms common predictors in the literature. The study highlights the efficiency and accuracy of the machine learning approach in this field. Yan et al. [32] compared BPNN and RBFNN models for predicting drag coefficients of non-spherical particles in gas–solid flow. The RBFNN model was found to be more effective, regardless of particle sphericity. The study provides valuable insights for fluidization studies. Mirvakili et al. [33] used ANNs to predict the terminal falling velocity of non-spherical particles in fluids. The ANN accurately predicted terminal velocities using 361 data points. This research offers a reliable

method to predict particle behavior in fluid dynamics. Agwu et al. [34] developed an ANN model to predict drill cuttings' settling velocity in wellbores. The model considers various shapes of cuttings and fluid properties, providing a more accurate and innovative approach to estimating settling velocity under real-world drilling conditions. Zhu et al. [35] compared three machine learning models to estimate sediment settling velocity. The decision tree (DT) model outperformed other models and traditional methods in predicting velocity for sand and gravel. Advanced modeling techniques can further improve estimation methods. Maiti et al. [36] developed an empirical correlation to predict the settling velocity of solids in non-Newtonian liquids using experimental methods and ANN modeling. The study confirmed the effectiveness of ANN techniques in predicting settling velocity more accurately than previous methods. Rushd et al. [37] used machine learning to predict settling velocity and found support vector regression with a polynomial kernel to be the most effective method. Their model was validated through rigorous statistical methods on 967 fluid samples, highlighting the potential of AI in fluid dynamics. In follow-up research, they used a large dataset to evaluate machine learning models for predicting the settling velocity of particles in Newtonian fluids, offering a more accurate and reliable method using advanced AI techniques. Zhu et al. [28] developed ANN models to predict proppant settling velocity and orientation in vertical fractures. Based on 588 experiments, they analyzed the impact of proppant shape, fluid properties, and fracture wall effects on the settling characteristics. The insights we gained can improve hydraulic fracturing performance. Rushd et al. [38] used AI to predict the settling velocity of spherical and non-spherical particles. Their detailed dataset improved accuracy and reliability. This study applied AI in a field that typically relies on empirical and experimental methods. Cahyono [39] developed seven equations using artificial neural network (ANN) methodology to predict the settling velocity of sediment particles. Data were sourced from digitized charts by the U.S. Interagency Committee on Water Resources, and the equations were compared with existing ones for validation. This presents a new approach in sedimentology for predicting settling velocities.

Table 1. Studies on prediction of drag coefficient and settling velocity of particles using AI technology.

Authors	AI Model	Number of Data Points	Fluid	Particle	Input Parameters	Predicted Parameter
Rooki et al. [30]	ANN	88 (63 train, 25 test)	Newt, PL	Spherical	ρ_f, ρ_p, d_p, K, n	U_p
Goldstein and Coco [31]	GP	985 (40 train, 472 validation, 473 test)	Newt	Non-spherical	d_p, ν, R	U_p
Yan et al. [32]	BPNN, RBFNN	—	Newt	Spherical, Non-spherical	—	C_D
Agwu et al. [34]	ANN	336 (236 train, 50 test, 50 validation)	Newt	Spherical, Non-spherical	Φ, ρ_p, d_p, μ, ρ_f	U_p
Zhu et al. [35]	FFNN, DL, DT	756 (529 train, 227 test)	Newt	Non-spherical	d_p, ν, R	U_p
Maiti et al. [36]	ANN	54 (38 train, 11 validation, 5 test)	PL	Non-spherical	n, K, ρ_f, ϕ, d_p, d_t	U_p

Table 1. *Cont.*

Authors	AI Model	Number of Data Points	Fluid	Particle	Input Parameters	Predicted Parameter
Rushd et al. [37]	SVR-RBF, SVR-P, SVR-L, RFR, SGB, BART, KNN, MLP, ANN	967 (774 train, 193 test)	Newt, Bin, PL, HB	Spherical	d_p, ρ_p, ρ_f, τ_y, K, n	U_p
Rushd et al. [40]	Gaussian processes, MLP, RBF, M5′ model tree, RF	3328 (2330 train, 998 test)	Newt, Bin, PL, HB	SphericalNon-spherical	d_p, Φ, ρ_p, ρ_f, τ_y, K, n	U_p
Zhu et al. [28]	ANN	588 (470 train, 118 test)	PL	Non-spherical	ρ_p, d, L_p, K, n, W, ρ_f	U_p
Rushd et al. [38]	ANN, SVM, KNN, PR, DT, RF	2726 (2181 train, 545 test)	Newt	SphericalNon-spherical	d_p, ρ_p, Φ, ρ_f, μ	U_p

Implementing AI, particularly ANN, in predicting settling velocity is motivated by several factors. (1) ANN can handle a broader range of variables and interactions, making them suitable for complex systems. (2) AI can uncover patterns and relationships in data that might not be apparent or easily modeled through traditional methods. (3) Once trained, AI models can provide rapid predictions, which is beneficial in practical applications. AI offers enhanced predictive accuracy, especially in systems where interactions are nonlinear and multifaceted, such as in the settling of non-spherical particles in non-Newtonian fluids. The ability of AI to learn from data allows it to adapt to various conditions without the need to re-derive formulas or extensively recalibrate models. However, these studies have limitations in terms of particle shape and fluid type. For instance, some models are only suitable for spherical particles [30,37] or Newtonian fluids [31,32,34,35,38], while others are only applicable to non-spherical particles in power-law fluids [28,36]. Moreover, some studies lack experimental data for non-spherical particles in non-Newtonian fluids [40], making it difficult to predict their settling velocity. Therefore, developing an AI model to accurately predict spherical and non-spherical particles' settling velocity in Newtonian and non-Newtonian fluids is crucial in petroleum engineering. In this paper, we aim to achieve the following objectives: (1) developing an ANN model to accurately predict the settling velocity of both spherical and non-spherical particles in both Newtonian and non-Newtonian fluids, (2) incorporating the impact of particle settling orientation in the prediction of settling velocity, and (3) performing a sensitivity analysis on the various input parameters of the proposed ANN model to evaluate their individual effects on settling velocity prediction.

2. Dataset

2.1. Particle Settling Experiments

The details of the particle settling experiments are provided in three papers published by our team [16,29,41]. The experimental setup for particle settling included a 1.5 m height tube, a high-speed camera, and a computer for data acquisition. A total of 114 particles, varying in density, shape, and size, were used. Both Newtonian and non-Newtonian fluids were employed, as shown in Table 2. Please refer to the Supplementary Materials File S1 for a comprehensive dataset comprising a total of 931 experimental data points.

Table 2. Experimental matrix of particle settling.

Particle Properties		Fluid Properties		
Shape (Sphericity)	ρ_p **(kg/m^3)**	**Fluid Type**	**Rheology**	
			***K* (Pa·s^n)**	***n***
Sphere (1) Cube (0.806) Cylinder (0.697, 0.779, 0.640) Disk (0.756, 0.873, 0.471)	2680 4450 7960	Newtonian	0.066	1
			0.124	1
			0.135	1
			0.289	1
			0.6685	1
		Power-law	0.260	0.755
			1.202	0.650
			3.233	0.576
			5.028	0.548
			9.608	0.505

The dataset comprising 931 experimental data points was meticulously collected under controlled laboratory conditions. Each experiment was repeated multiple times to ensure consistency and to minimize experimental errors. The range of experimental conditions was chosen to represent a wide spectrum of scenarios encountered in particle dynamics, particularly in petroleum engineering contexts. It should be noted that uncertainties in data acquisition are inevitable in any experimental process. These uncertainties may arise from various sources, such as measurement errors (e.g., in the measurement of particle size or fluid properties), environmental conditions, and intrinsic variations in the materials used. To address these issues, experiments are conducted under consistent environmental conditions. Moreover, multiple repetitions are performed for each experimental condition to help average out random errors.

Figure 1 demonstrates that various non-spherical particles differ in settling orientation, with some particles even changing orientation during settling. At low Reynolds numbers, the initial settling orientation remains consistent, while at high Reynolds numbers, the settling orientation changes continuously throughout the settling process, making it more complex.

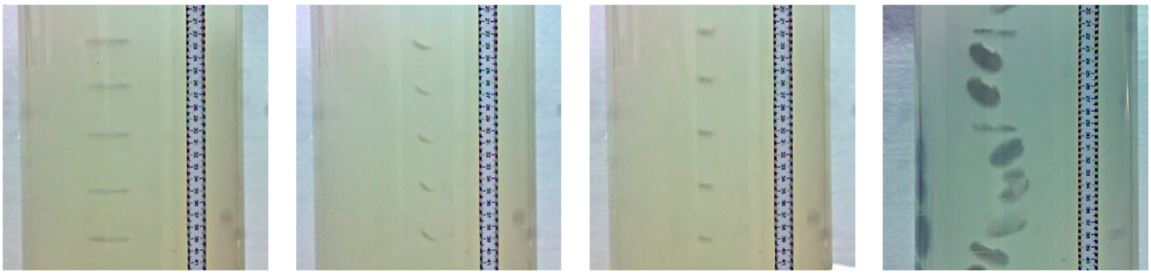

(**a**) (**b**) (**c**) (**d**)

Figure 1. Successive settling process of non-spherical particles with varying shapes and orientations (based on our previous experiments. (**a**): cylinder-shaped particle with 20 mm diameter and 5 mm height, (**b**): cylinder-shaped particle with 18 mm diameter and 6 mm height, (**c**): cube-shaped particle with 8 mm length, (**d**): cylinder-shaped particle settling with 30 mm diameter and 3 mm height).

2.2. Dataset Characteristics and Analysis

Table 3 and Figure 2 provide an intuitive display of the experimental data points for spherical and non-spherical particles in both Newtonian and non-Newtonian fluids. The data points are well balanced in this study, with 378 and 553 data points in Newtonian and non-Newtonian fluids, respectively. Notably, this dataset includes non-spherical particles in power-law fluids, which is a significant contribution to the literature. In contrast, Rushd et al. [40] utilized 3328 data points, but the majority are in Newtonian fluids (2732 data

points, 82%). Consequently, the AI model's features are primarily extracted from Newtonian fluids in that study. Furthermore, Rushd et al. [40] did not provide settling velocity data for non-spherical particles in non-Newtonian fluids, indicating that all data for non-spherical particles are in Newtonian fluids.

Table 3. Data point numbers for different particles in different fluids of this study.

Particle	Fluid	Data Point Number
Spherical	Newtonian	102
Non-spherical	Newtonian	276
Spherical	Power-law	98
Non-spherical	Power-law	455
Total		931

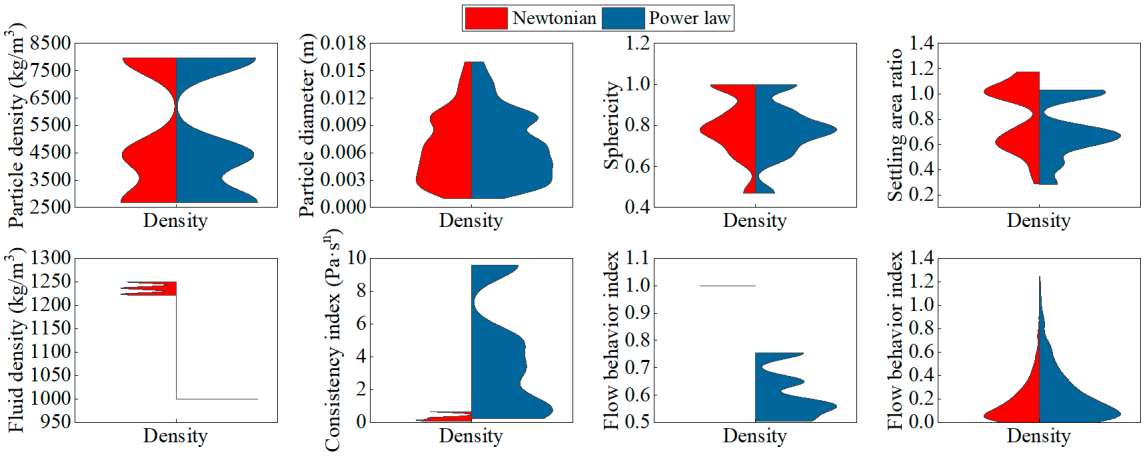

Figure 2. Input parameter density distribution and box plot for predicting particle settling velocity in Newtonian and power-law fluids.

It could be found from Table 3 and Figure 2 that there is an imbalance in these data towards non-spherical samples in non-Newtonian fluids. This was primarily due to the following three reasons. (1) Experimental constraints: All data used were obtained from our experiments. Non-spherical particles, due to their varied shapes and sizes, inherently require more experimental observations compared to spherical ones. Similarly, characterizing non-Newtonian fluids, represented by multiple parameters like consistency index and flow behavior index, necessitate more extensive experimental setups. (2) Focus on underrepresented areas: This study particularly aimed to address the less-explored domain of non-spherical particles in non-Newtonian fluids, prevalent in petroleum engineering. Although spherical particles and Newtonian fluids were included for comparative analysis and to broaden the model's applicability, our primary focus was on more complex scenarios. (3) Existing literature: There are abundant research and highly accurate predictive formulas available for spherical particles in Newtonian fluids, which guided our decision to focus on areas with less available data.

3. Methodology

3.1. Data Preparation and Partitioning

This study primarily focused on parameters that significantly influence particle settling velocity in both Newtonian and non-Newtonian fluids. The input data included particle characteristics (like size, density, and shape), fluid properties (such as density and viscosity), and flow dynamics parameters. These types of data were selected based on their recognized impact on settling behavior, as documented in the existing fluid dynamics literature. The criteria for selecting specific input variables were based on several factors. (1) Each variable

was chosen for its direct or indirect impact on particle settling velocity, as supported by previous research findings. (2) The variables selected were measurable and available within the scope of experimental capabilities. (3) To ensure the model's applicability across different scenarios, a diverse range of variables representing various particle types and fluid conditions was selected. (4) The selection was also influenced by the feasibility and reliability of accurately measuring each variable under laboratory conditions.

The dataset of particle settling velocity is partitioned into two sets: a train set used to adjust the weights and biases in the ANN model and a test set used to independently evaluate the performance of the model. Following previous research, 80% of the dataset is allocated to the train set, while the remaining 20% is assigned to the test set. As shown in Table 4, the statistical properties of the train and test sets are similar.

Table 4. Statistical parameters of train and test sets for the ANN model.

Model Variables and Datasets		Statistical Parameters			
		Mean	Standard Deviation	Min	Max
Particle density (kg/m^3)	Train set	4961	2680	2171	7960
	Test set	5243	2680	2303	7960
Particle equivalent diameter (m)	Train set	0.00678	0.001	0.00377	0.01594
	Test set	0.00665	0.001	0.00363	0.01594
Sphericity	Train set	0.793	0.471	0.149	1
	Test set	0.792	0.471	0.140	1
Settling area ratio	Train set	0.765	0.282	0.246	1.174
	Test set	0.749	0.282	0.234	1.174
Fluid density (kg/m^3)	Train set	1098	1000	116	1250
	Test set	1088	1000	114	1250
Consistency index ($Pa \cdot s^n$)	Train set	2.354	0.066	3.024	9.608
	Test set	2.705	0.066	3.293	9.608
Flow behavior index	Train set	0.771	0.505	0.204	1
	Test set	0.751	0.505	0.205	1

3.2. Development of the ANN Model

This study utilizes a three-layer ANN model with a common structure consisting of an input layer, a hidden layer, and an output layer. While adding more hidden layers may improve the model's performance, it also raises the potential for overfitting when dealing with a small dataset. Guided by the principle of Occam's Razor, where simpler models are preferred due to their generalizability and lower risk of overfitting, this study employs a one-hidden-layer ANN model. The input layer of the model includes seven nodes, with each node representing an input parameter that has an impact on the settling velocity of the particles. In the output layer, one node represents the particle settling velocity. However, determining the optimal number of nodes in the hidden layer is not guided by any theory and relies mainly on experience. The architecture of the ANN model is illustrated in Figure 3.

To train the ANN model for predicting settling velocity, we set the learning rate to 0.001 and used the mean squared error as the loss function. The hidden and output layers were activated using ReLU and Sigmoid functions, respectively. We trained the model for 1000 epochs to optimize its performance. In order to determine the optimal node number in the hidden layer, we minimized the difference between predicted and measured settling velocity. In our study, we indeed utilized K-fold cross-validation for training the model. Specifically, we employed 10-fold cross-validation, a standard machine learning approach, to ensure our model's robustness and generalizability. This method involved partitioning the dataset into ten equal-sized subsets. Each iteration used one subset as the

test set, while the remaining nine subsets were combined to form the training set. This process was repeated ten times, with each subset serving as the test set exactly once. The use of K-fold cross-validation allowed us to mitigate the potential biases associated with the random sampling of the training and test sets, thus enhancing the reliability of our model's performance assessment. The average R^2 value and the standard deviation of the R^2 values from these iterations provided a comprehensive measure of the model's predictive accuracy and consistency. Our results showed that the ANN model performed best when the hidden layer contains 42 nodes. These parameters were carefully chosen to ensure that the model was accurate and reliable in predicting settling velocity in various petroleum engineering applications.

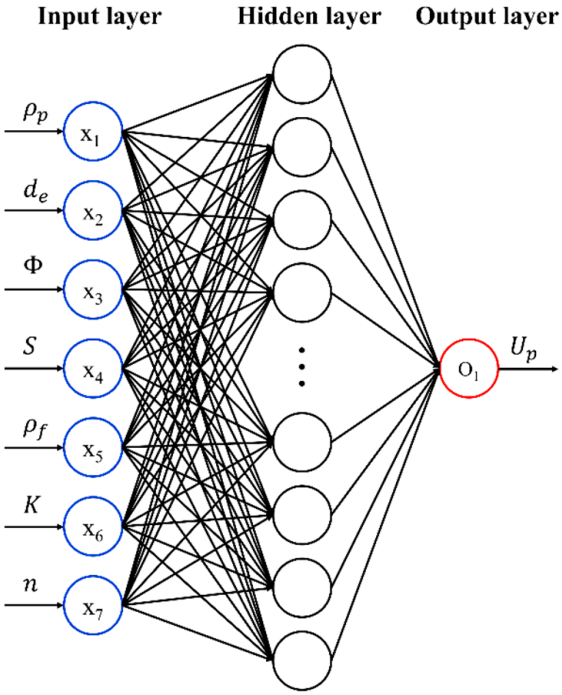

Figure 3. The architecture of the ANN model.

The accuracy of the proposed ANN model was assessed using the average absolute relative error (AARE) (Equation (1)), root mean square error (RMSE) (Equation (2)), and mean absolute error (MAE) (Equation (3)) between measured and predicted settling velocity.

Average absolute relative error (AARE):

$$\text{AARE} = \frac{1}{N}\sum_{i=1}^{n}\left|\frac{\hat{U}_{p,i} - U_{p,i}}{U_{p,i}}\right| \quad (1)$$

Root mean square error (RMSE):

$$\text{RMSE} = \sqrt{\frac{1}{N}\sum_{i=1}^{n}\left(\hat{U}_{p,i} - U_{p,i}\right)^2} \quad (2)$$

Mean absolute error (MAE):

$$\text{MAE} = \frac{1}{N}\sum_{i=1}^{n}\left|\hat{U}_{p,i} - U_{p,i}\right| \quad (3)$$

where $\hat{U}_{p,i}$ is the particle settling velocity predicted by the ANN model, $U_{p,i}$ is the measured particle settling **velocity**, and N is the total number of experimental data.

4. Results and Discussion

Table 5 and Figure 4 demonstrate that the average absolute relative error (AARE) in the train and test sets is 8.48% and 8.64%, respectively. To evaluate the impact of the settling area ratio, we compared the prediction accuracy of the ANN model with and without the input of the settling area ratio. Our findings show that the prediction accuracy could be enhanced by including the settling area ratio as an input, which validates that settling orientation is a critical factor affecting particle settling velocity. The weights and biases used in the ANN model are provided in Appendix A.

Table 5. Summary of ANN performance in train and test sets.

Models	Data Set	AARE	RMSE	MAE
ANN with input *S*	Train	0.0848	0.016	0.010
	Test	0.0864	0.026	0.015
ANN without input *S*	Train	0.1092	0.018	0.011
	Test	0.1022	0.026	0.016

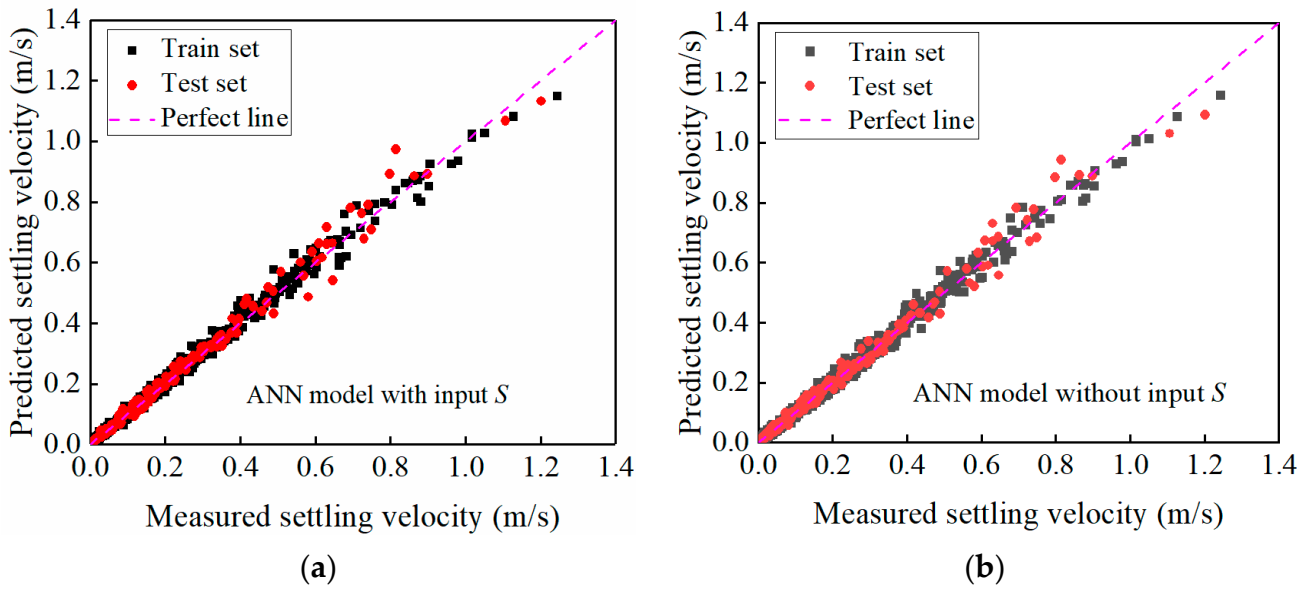

Figure 4. Comparison of predicted settling velocity by ANN model and measured settling velocity in train and test sets ((**a**) ANN model with input *S*; (**b**) ANN model without input *S*).

Table 6 and Figure 5 illustrate the accuracy of the proposed ANN model in comparison to other empirical correlations [16,29,42,43]. Although the model proposed by Song et al. [29] provides precise predictions in Newtonian fluids, it is unsuitable for power-law fluids. In contrast, the ANN model can accurately predict the settling velocity of both spherical and non-spherical particles in both Newtonian and power-law fluids.

Table 6. Comparison of ANN model with empirical correlations.

Model	AARE of Train Set		AARE of Test Set	
	Newtonian	Power-Law	Newtonian	Power-Law
Haider and Levenspiel [42]	15.47%	/	15.52%	/
Madhav and Chhabra [43]	/	89.14%	/	87.53%
Song et al. [29]	3.96%	/	3.89%	/
Xu et al. [16]	/	14.03%	/	13.85%
ANN model in this study	9.69%	7.63%	8.41%	8.79%

Note: '/' in Table 6 represents that this model is unsuitable for this fluid type.

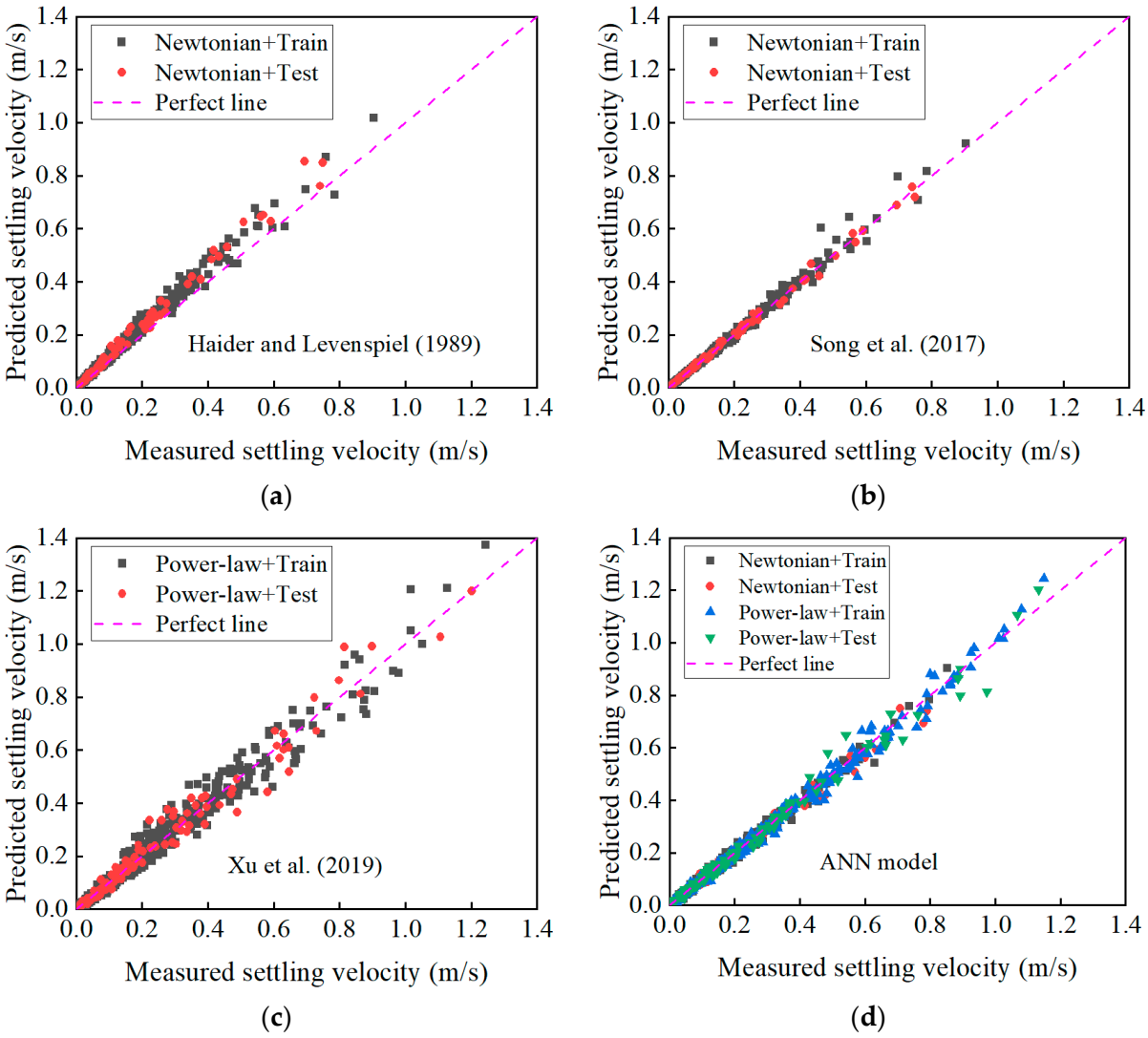

Figure 5. Comparison of settling velocity predictions by different models with measured values (**a**): Haider and Levenspiel [42], (**b**): Song et al. [29], (**c**): Xu et al. [16], (**d**): ANN model.

The inclusion of Newtonian fluid and spherical particle data slightly reduced the ANN model's precision compared to high-accuracy models specific to these conditions. However, it significantly enhanced the model's accuracy for non-Newtonian fluids. For instance, the prediction error for non-Newtonian fluids was markedly lower than existing models. In conclusion, while the dataset imbalance slightly affected the model's performance in predicting Newtonian fluid and spherical particle settling velocities, it considerably improved its applicability and accuracy for non-spherical particles in non-Newtonian fluids. As for the sensitivity of this imbalance, it could be found that an imbalance in the dataset can influence a model's performance and generalizability. These analyses involved testing the model's performance with varied proportions of spherical and non-spherical particles, as well as Newtonian and non-Newtonian fluids. The results indicated that while there is some sensitivity to these variations, the overall predictive accuracy of the model remained robust across different scenarios. This suggests that the proposed model can generalize well despite the uneven distribution of data points.

To compare with other advanced algorithms, K-fold cross-validation (K = 10) is used to determine the most suitable model for this study. The evaluation focused on the coefficient of determination as a measure of model accuracy, defined as Equation (4):

$$R^2 = \frac{SS_{\text{regression}}}{SS_{\text{total}}} \tag{4}$$

where $SS_{\text{regression}}$ is the regression sum of squares, representing the fit error of the regression model, and SS_{total} is the total sum of squares, indicating the dispersion of the total data. Different machine learning algorithms were trained and tested for a comparative analysis with the ANN model, including DT [44], RFR [45], XGBOOST [46], KNN [47], and SVM [48]. The results of this evaluation are summarized in Table 7, which shows the average values and standard deviations for six models obtained through K-fold cross-validation. The findings indicate that the ANN model exhibits high accuracy and relative stability. Based on these results, the ANN model is used for further research.

Table 7. Model accuracy compared with other models.

Models	Average R^2 Value from K-Fold Cross-Validation	Standard Deviation of R^2 Values from K-Fold Cross-Validation
DT	0.8016	0.0580
RFR	0.9374	0.0112
XGBOOST	0.9679	0.0093
KNN	0.8922	0.0204
SVM	0.9083	0.0287
ANN (one-hidden-layer)	0.9706	0.0085

Using advanced models like SVR could obtain higher accuracy; however, considering the broader context of our research and its specific objectives, the ANN model is used for the following reasons: (1) Consistency with initial research design: this study was initially conceptualized and executed with an ANN-based approach and was structured around this methodology. (2) Balance between accuracy and complexity: while the SVR model showed marginally better performance, the ANN model still provides high accuracy. Additionally, ANN offers a balance between predictive power and model interpretability, which aligns with our research aims. (3) Scope of study: comprehensive revisions to include a different AI model would require substantial changes in the analysis and the manuscript's narrative, which might shift the focus away from the original scope of our research.

The calculation method proposed by Agwu et al. [34], known as the connection weights algorithm, is demonstrated in Equation (5). It involves summing the products of weights associated with the connections among input, hidden, and output layers in ANN model.

$$RI_x = \sum_{y=1}^{M} w_{xy} w_{yz} \tag{5}$$

where RI_x is the relative importance of input variable x, M is the total number of hidden neurons, w_{xy} is the weight of the connection between input and hidden layers, and w_{yz} represents the weight of the connection between hidden and output layers.

Figure 6 displays the relative importance of different input variables on particle settling velocity. The consistency index (x_6) has the greatest impact, followed by the particle diameter (x_2), fluid density (x_5), settling area ratio (x_4), particle density (x_1), flow behavior index (x_7), and sphericity (x_3). The absolute values determine the importance, whereas the sign (positive or negative) indicates the direction of the effect of each input on the output. As depicted in Figure 6, an increase in the consistency index, settling area ratio, and fluid density results in a decrease in particle settling velocity. Conversely, an increase in particle diameter, particle density, flow behavior index, and sphericity lead to an increase in particle settling velocity. An increase in particle density (x_1) results in

a higher gravitational force, leading to an increased settling velocity. A larger particle diameter (x_2) also increases gravitational force, enhancing the settling velocity. The cubic relationship between diameter and volume implies a stronger positive influence of diameter compared to density. As sphericity (x_3) increases, particles become more sphere-like, thus increasing their settling velocity. However, this effect is less pronounced due to minor variations in sphericity within our experimental data range. A larger settling area ratio (x_4) increases the cross-sectional area facing resistance, thus significantly impacting the settling velocity. Higher fluid density (x_5) generates greater buoyancy, reducing the settling velocity of particles. The consistency index (x_6) relates to the viscosity in non-Newtonian fluids. A higher consistency index means greater resistance, significantly affecting the settling velocity. Higher flow behavior index values indicate a closer resemblance to Newtonian fluids, showing a positive correlation with settling velocity.

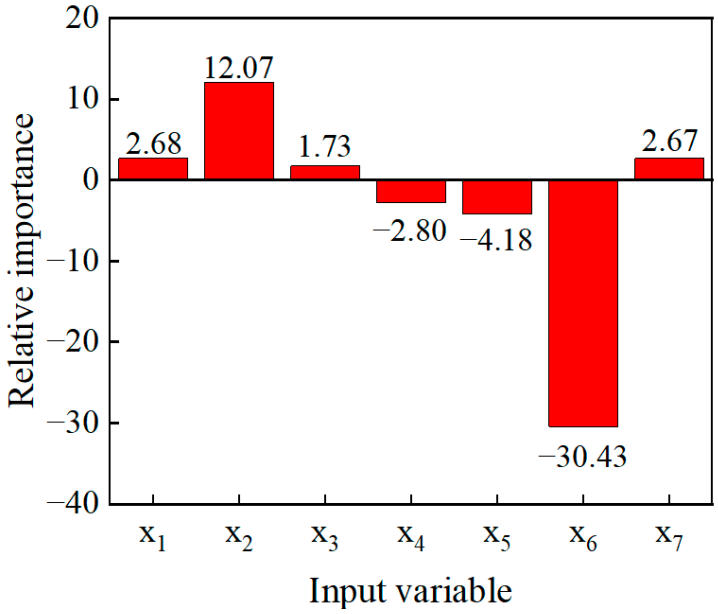

Figure 6. Relative importance of input variables in the ANN model for predicting particle settling velocity.

5. Conclusions

In this study, we successfully developed an ANN model for predicting the settling velocity of both spherical and non-spherical particles in various fluid environments. Utilizing an extensive dataset of 931 data points, we demonstrated the robustness and accuracy of the model. Key achievements of our research include:

(1) The development of an ANN model structured as 7-42-1, which achieved an average absolute relative error of 8.51%, highlighting its precision in predicting settling velocities.

(2) A detailed assessment of the impact of each input variable on the settling velocity revealed the consistency index to be the most negatively impactful factor, while particle diameter showed the greatest positive influence.

(3) The proposed model's predictions for particle settling velocities were reasonably accurate for both spherical and non-spherical particles in Newtonian and non-Newtonian fluids, showcasing its effectiveness when compared to empirical models.

Supplementary Materials: The following supporting information can be downloaded at: https://www.mdpi.com/article/10.3390/app14020826/s1. File S1: Experimental data of particle settling velocity-931 data.xlsx.

Author Contributions: Conceptualization, W.L. and X.S.; methodology, W.L. and Z.X.; validation, X.J.; formal analysis, X.J.; investigation, J.L.; resources, Z.X.; data curation, J.L.; writing—original draft

preparation, Z.X.; writing—review and editing, S.D.; visualization, Z.X.; supervision, S.D.; project administration, W.L.; funding acquisition, W.L. All authors have read and agreed to the published version of the manuscript.

Funding: This research was funded by the National Natural Science Foundation of China (No. 52104009), China National Petroleum Corporation Scientific Research and Technology Development Project "200C/105MPa Continuous tube drilling and grinding/Jet operation Tool Development" (No. 2020B-4018), and China National Petroleum Corporation Limited major technology promotion project "Full series Continuous pipe operation Technology Promotion" (No. 2022ZT01).

Data Availability Statement: The original contributions presented in the study are included in the Supplementary Material, further inquiries can be directed to the corresponding author.

Conflicts of Interest: Authors Weiping Lv, Xia Jia, Jiawei Liu were employed by the Jianghan Machinery Research Institute Limited Company of CNPC. The remaining authors declare that the research was conducted in the absence of any commercial or financial relationships that could be construed as a potential conflict of interest. The authors declare no conflicts of interest.

Nomenclature

C_D	drag coefficient
d_p	particle diameter, m
d_t	column diameter, m
K	consistency index of power-law fluid, Pa·s^n
L_p	length of rod particle, m
M	total number of hidden neurons
n	flow behavior index of power-law fluid
N	total number of experimental data
R	submerged specific gravity
Re	particle Reynolds number
RI_x	relative importance of input variable x
S	settling area ratio
U_p	particle settling velocity, m/s
$\hat{U}_{p,i}$	predicted particle settling velocity
$U_{p,i}$	measured particle settling velocity
W	fracture width, m
w_{xy}	weight of the connection between input and hidden layers
w_{yz}	weight of the connection between hidden and output layers
x_1	particle density
x_2	particle diameter
x_3	sphericity
x_4	settling area ratio
x_5	fluid density
x_6	consistency index
x_7	flow behavior index
Greek letters	
Φ	sphericity
ρ_f	fluid density, kg/m^3
ρ_p	particle density, kg/m^3
ν	kinematic viscosity of fluid, m^2/s
μ	viscosity of Newtonian fluid, Pa·s
τ_y	yield stress, Pa
Abbreviations	
AARE	average absolute relative error
AI	artificial intelligence
ANN	artificial neural network
BART	Bayesian additive regression tree
Bin	Bingham fluid

BPNN	back propagation neural network
DL	deep learning
DT	decision tree
FFNN	feed forward neural network
HB	Herschel–Bulkley fluid
KNN	K-nearest neighbor
GP	genetic programming
MAE	mean absolute error
MLP	multilayer perceptron
Newt	Newtonian fluid
PL	power-law fluid
PR	polynomial regression
RBF	radial basis function
RBFNN	radial basis function neural network
RF	random forest
RFR	random forest regression
RMSE	root mean square error
SGB	stochastic gradient boosting
SVM	support vector machine
SVR-L	support vector regression with linear
SVR-P	support vector regression with polynomial
SVR-RBF	support vector regression with radial basis function

Appendix A Weights and Biases of the ANN Model for Particle Settling Velocity

Table A1. Weights and biases of the ANN model for particle settling velocity.

Hidden Layer Neuron	Input Layer Weights							Input Layer Bias	Hidden Layer Weights	Hidden Layer Bias
	ρ_p	d_e	Φ	S	ρ_f	K	n			
h1	−0.469	0.213	−0.423	0.002	0.201	−0.894	−0.071	−0.170	0.866	−0.145
h2	0.104	−0.211	−0.125	−0.408	0.169	0.182	−0.018	0.583	−0.778	
h3	0.361	0.899	0.770	0.268	0.001	−0.238	−0.060	−0.256	1.008	
h4	−0.150	−0.378	0.701	0.371	0.717	0.081	−0.475	−0.262	−1.063	
h5	−0.017	−0.371	−0.249	0.241	−0.146	0.025	0.168	−0.101	0.134	
h6	−0.488	−0.419	0.034	0.008	0.038	−2.229	0.366	0.008	0.376	
h7	0.226	0.448	0.311	0.202	0.142	0.004	−0.116	−0.146	0.301	
h8	0.107	−0.140	−0.321	0.021	0.303	0.016	−0.346	−0.045	0.291	
h9	−0.057	−0.085	0.084	0.185	−0.032	−0.018	0.092	0.139	−0.159	
h10	−0.112	−0.187	−0.020	0.124	−0.048	−6.756	0.428	−0.059	1.579	
h11	0.079	0.173	−0.665	−0.052	0.425	−0.099	−0.163	0.465	−1.203	
h12	0.358	−0.814	−0.449	−0.242	0.399	0.524	0.057	0.733	−0.696	
h13	−0.086	−0.293	−0.234	0.115	0.082	−0.305	0.076	−0.084	0.295	
h14	0.453	−0.457	0.117	−0.766	−0.052	0.120	0.119	−0.036	1.323	
h15	−0.603	0.605	−0.084	0.147	0.401	−0.012	−0.020	0.133	−0.842	
h16	0.179	0.374	0.079	−0.017	−0.189	0.185	0.242	−0.137	0.209	
h17	0.012	−0.336	−0.317	0.045	−0.298	0.088	−0.284	0.000	−0.109	
h18	0.446	−0.936	0.026	−0.021	−0.132	−0.095	−0.124	0.312	−0.579	
h19	0.075	−0.262	−0.455	0.158	−0.506	0.036	0.043	0.367	−0.993	
h20	−0.412	−0.821	−0.047	−0.149	0.057	0.595	0.259	0.091	−1.560	
h21	−0.184	0.002	0.225	0.221	0.001	0.382	0.213	0.121	−0.084	
h22	−0.230	−0.321	−0.313	0.139	0.045	−0.169	−0.348	0.000	−0.188	
h23	0.304	−0.061	0.083	0.210	0.153	−0.140	0.008	0.129	−0.275	
h24	−0.065	−1.518	0.311	−0.002	−0.110	−0.192	−0.217	0.622	−1.151	
h25	−0.024	−0.338	−0.264	−0.054	0.066	−3.483	0.599	0.095	1.548	
h26	−0.219	−0.704	−0.084	0.453	0.553	0.870	−0.076	0.372	−0.830	
h27	−0.239	0.068	0.273	−0.297	−0.331	−0.283	−0.321	0.000	−0.095	
h28	−0.010	−2.243	−0.082	−0.021	0.088	0.370	−0.002	0.326	−2.814	

Table A1. *Cont.*

Hidden Layer Neuron	Input Layer Weights							Input Layer Bias	Hidden Layer Weights	Hidden Layer Bias
	ρ_p	d_e	Φ	S	ρ_f	K	n			
h29	−0.118	−0.158	0.391	−0.762	−0.252	0.072	0.272	0.130	1.900	
h30	0.022	0.125	0.562	0.436	0.082	−0.760	0.101	−0.219	0.473	
h31	−0.074	0.283	0.461	0.404	0.057	−0.176	−0.254	−0.360	0.514	
h32	−0.089	0.243	−0.205	−0.913	0.191	−0.155	−0.232	0.367	1.113	
h33	−0.996	0.341	0.251	−0.039	−0.234	−0.320	−0.220	0.503	−1.164	
h34	−0.211	−0.441	0.153	0.078	0.365	−0.045	−0.130	0.454	−1.031	
h35	0.191	0.077	0.239	0.246	0.045	−0.926	0.156	−0.198	0.515	
h36	0.193	−0.336	0.114	−0.290	−0.323	−0.093	−0.161	−0.069	0.078	
h37	−0.168	−0.167	0.349	0.082	0.460	0.368	−0.416	0.051	−0.861	
h38	−0.038	−0.233	−0.309	−0.343	−0.269	−0.228	−0.032	0.000	0.054	
h39	0.149	−0.041	0.268	0.180	−0.410	−5.645	0.373	−0.302	1.799	
h40	0.118	−0.262	0.113	−0.180	−0.325	0.667	−1.171	−0.167	1.072	
h41	0.120	−1.208	0.386	−0.026	0.378	−0.627	0.173	−0.025	−1.049	
h42	−0.037	0.092	−0.286	0.256	0.364	0.327	0.051	0.145	−0.352	

References

1. Wang, X.; Gong, L.; Li, Y.; Yao, J. Developments and applications of the CFD-DEM method in particle–fluid numerical simulation in petroleum engineering: A review. *Appl. Therm. Eng.* **2023**, *222*, 119865. [CrossRef]
2. Busch, A.; Johansen, S.T. Cuttings transport: On the effect of drill pipe rotation and lateral motion on the cuttings bed. *J. Pet. Sci. Eng.* **2020**, *191*, 107136.
3. Huque, M.M.; Rahman, M.A.; Zendehboudi, S.; Butt, S.; Imtiaz, S. Experimental and numerical study of cuttings transport in inclined drilling operations. *J. Pet. Sci. Eng.* **2022**, *208*, 109394. [CrossRef]
4. Shahsavari, M.H.; Khamehchi, E.; Fattahpour, V.; Molladavoodi, H. Investigation of sand production prediction shortcomings in terms of numerical uncertainties and experimental simplifications. *J. Pet. Sci. Eng.* **2021**, *207*, 109147. [CrossRef]
5. Nouri, A.; Vaziri, H.; Belhaj, H.; Islam, M.R. Comprehensive transient modeling of sand production in horizontal wellbores. *SPE J.* **2007**, *12*, 468–474. [CrossRef]
6. Barboza, B.R.; Chen, B.; Li, C. A review on proppant transport modelling. *J. Pet. Sci. Eng.* **2021**, *204*, 108753.
7. Sahai, R.; Moghanloo, R.G. Proppant transport in complex fracture networks—A review. *J. Pet. Sci. Eng.* **2019**, *182*, 106199. [CrossRef]
8. GhasemiKafrudi, E.; Hashemabadi, S.H. Numerical study on cuttings transport in vertical wells with eccentric drillpipe. *J. Pet. Sci. Eng.* **2016**, *140*, 85–96.
9. Minakov, A.V.; Zhigarev, V.A.; Mikhienkova, E.I.; Neverov, A.L.; Buryukin, F.A.; Guzei, D.V. The effect of nanoparticles additives in the drilling fluid on pressure loss and cutting transport efficiency in the vertical boreholes. *J. Pet. Sci. Eng.* **2018**, *171*, 1149–1158. [CrossRef]
10. Wu, C.-H.; Sharma, M.M. Modeling proppant transport through perforations in a horizontal wellbore. *SPE J.* **2019**, *24*, 1777–1789. [CrossRef]
11. Huque, M.M.; Rahman, M.A.; Zendehboudi, S.; Butt, S.; Imtiaz, S. Investigation of cuttings transport in a horizontal well with high-speed visualization and electrical resistance tomography technique. *J. Nat. Gas Sci. Eng.* **2021**, *92*, 103968.
12. Dankers, P.J.T.; Winterwerp, J.C. Hindered settling of mud flocs: Theory and validation. *Cont. Shelf Res.* **2007**, *27*, 1893–1907. [CrossRef]
13. Koo, S. Estimation of hindered settling velocity of suspensions. *J. Ind. Eng. Chem.* **2009**, *15*, 45–49.
14. Cheng, N.-S. Comparison of formulas for drag coefficient and settling velocity of spherical particles. *Powder Technol.* **2009**, *189*, 395–398.
15. Chhabra, R.P. *Bubbles, Drops, and Particles in Non-Newtonian Fluids*; CRC Press: Boca Raton, FL, USA, 2006.
16. Xu, Z.; Song, X.; Li, G.; Pang, Z.; Zhu, Z. Settling behavior of non-spherical particles in power-law fluids: Experimental study and model development. *Particuology* **2019**, *46*, 30–39. [CrossRef]
17. Corey, A.T. *Influence of Shape on the Fall Velocity of Sand Grains*; Colorado A & M College: Fort Collins, CO, USA, 1949.
18. Zhu, X.; Zeng, Y.H.; Huai, W.X. Settling velocity of non-spherical hydrochorous seeds. *Adv. Water Resour.* **2017**, *103*, 99–107. [CrossRef]
19. Chien, S.-F. Settling velocity of irregularly shaped particles. *SPE Drill. Complet.* **1994**, *9*, 281–289. [CrossRef]
20. Johnson, D.L.; Leith, D.; Reist, P.C. Drag on non-spherical, orthotropic aerosol particles. *J. Aerosol Sci.* **1987**, *18*, 87–97.
21. Gunes, D.Z.; Scirocco, R.; Mewis, J.; Vermant, J. Flow-induced orientation of non-spherical particles: Effect of aspect ratio and medium rheology. *J. Non-Newton. Fluid Mech.* **2008**, *155*, 39–50.

22. Hölzer, A.; Sommerfeld, M. New simple correlation formula for the drag coefficient of non-spherical particles. *Powder Technol.* **2008**, *184*, 361–365. [CrossRef]
23. Mandø, M.; Rosendahl, L. On the motion of non-spherical particles at high Reynolds number. *Powder Technol.* **2010**, *202*, 1–13.
24. Mele, D.; Dellino, P.; Sulpizio, R.; Braia, G. A systematic investigation on the aerodynamics of ash particles. *J. Volcanol. Geotherm. Res.* **2011**, *203*, 1–11. [CrossRef]
25. Zastawny, M.; Mallouppas, G.; Zhao, F.; van Wachem, B. Derivation of drag and lift force and torque coefficients for non-spherical particles in flows. *Int. J. Multiph. Flow* **2012**, *39*, 227–239. [CrossRef]
26. Dogonchi, A.S.; Hatami, M.; Hosseinzadeh, K.; Domairry, G. Non-spherical particles sedimentation in an incompressible Newtonian medium by Padé approximation. *Powder Technol.* **2015**, *278*, 248–256.
27. Bagheri, G.; Bonadonna, C. On the drag of freely falling non-spherical particles. *Powder Technol.* **2016**, *301*, 526–544.
28. Zhu, Z.; Song, X.; Li, G.; Xu, Z.; Zhu, S.; Yao, X.; Jing, S. Prediction of the settling velocity of the rod-shaped proppant in vertical fracture using artificial neural network. *J. Pet. Sci. Eng.* **2021**, *200*, 108158. [CrossRef]
29. Song, X.; Xu, Z.; Li, G.; Pang, Z.; Zhu, Z. A new model for predicting drag coefficient and settling velocity of spherical and non-spherical particle in Newtonian fluid. *Powder Technol.* **2017**, *321*, 242–250.
30. Rooki, R.; Doulati Ardejani, F.; Moradzadeh, A.; Kelessidis, V.C.; Nourozi, M. Prediction of terminal velocity of solid spheres falling through Newtonian and non-Newtonian pseudoplastic power law fluid using artificial neural network. *Int. J. Miner. Process.* **2012**, *110–111*, 53–61.
31. Goldstein, E.B.; Coco, G. A machine learning approach for the prediction of settling velocity. *Water Resour. Res.* **2014**, *50*, 3595–3601. [CrossRef]
32. Yan, S.; He, Y.; Tang, T.; Wang, T. Drag coefficient prediction for non-spherical particles in dense gas–solid two-phase flow using artificial neural network. *Powder Technol.* **2019**, *354*, 115–124. [CrossRef]
33. Mirvakili, A.; Roohian, H.; Chahibakhsh, S. Artifcial neural network approach for the prediction of terminal falling velocity of non-spherical particles through Newtonian and non-Newtonian fluids. *J. Oil Gas Petrochem. Technol.* **2019**, *6*, 1–14.
34. Agwu, O.E.; Akpabio, J.U.; Dosunmu, A. Artificial neural network model for predicting drill cuttings settling velocity. *Petroleum* **2020**, *6*, 340–352. [CrossRef]
35. Zhu, S.; Hrnjica, B.; Dai, J.; Sivakumar, B. Machine learning approaches for estimation of sediment settling velocity. *J. Hydrol.* **2020**, *586*, 124911. [CrossRef]
36. Maiti, S.B.; Bar, N.; Das, S.K. Terminal settling velocity of solids in the pseudoplastic non-Newtonian liquid system–Experiment and ANN modeling. *Chem. Eng. J. Adv.* **2021**, *7*, 100136. [CrossRef]
37. Rushd, S.; Hafsa, N.; Al-Faiad, M.; Arifuzzaman, M. Modeling the settling velocity of a sphere in Newtonian and Non-Newtonian fluids with machine-learning algorithms. *Symmetry* **2021**, *13*, 71.
38. Rushd, S.; Rahman, M.; Arifuzzaman, M.; Aktaruzzaman, M. A decision support system for predicting settling velocity of spherical and non-spherical particles in Newtonian fluids. *Part. Sci. Technol.* **2022**, *40*, 609–619. [CrossRef]
39. Cahyono, M. The development of explicit equations for estimating settling velocity based on artificial neural networks procedure. *Hydrology* **2022**, *9*, 98. [CrossRef]
40. Rushd, S.; Parvez, M.T.; Al-Faiad, M.A.; Islam, M.M. Towards optimal machine learning model for terminal settling velocity. *Powder Technol.* **2021**, *387*, 95–107.
41. Xu, Z.; Song, X.; Li, G.; Liu, Q.; Pang, Z.; Zhu, Z. Predicting fiber drag coefficient and settling velocity of sphere in fiber containing Newtonian fluids. *J. Pet. Sci. Eng.* **2017**, *159*, 409–418.
42. Haider, A.; Levenspiel, O. Drag coefficient and terminal velocity of spherical and nonspherical particles. *Powder Technol.* **1989**, *58*, 63–70.
43. Madhav, G.V.; Chhabra, R.P. Settling velocities of non-spherical particles in non-Newtonian polymer solutions. *Powder Technol.* **1994**, *78*, 77–83. [CrossRef]
44. Song, Y.Y.; Lu, Y. Decision tree methods: Applications for classification and prediction. *Shanghai Arch Psychiatry* **2015**, *27*, 130–135.
45. Zahedi, P.; Parvandeh, S.; Asgharpour, A.; McLaury, B.S.; Shirazi, S.A.; McKinney, B.A. Random forest regression prediction of solid particle erosion in elbows. *Powder Technol.* **2018**, *338*, 983–992. [CrossRef]
46. Chen, T.; Guestrin, C. XGBoost: A scalable tree boosting system. In Proceedings of the 22nd ACM SIGKDD International Conference on Knowledge Discovery and Data Mining, San Francisco, CA, USA, 13–17 August 2016; Association for Computing Machinery: San Francisco, CA, USA, 2016; pp. 785–794.
47. Zhang, S.; Li, X.; Zong, M.; Zhu, X.; Cheng, D. Learning k for kNN classification. *ACM Trans. Intell. Syst. Technol.* **2017**, *8*, 43.
48. Jian-xiong, D.; Krzyzak, A.; Suen, C.Y.; Fast, S.V.M. training algorithm with decomposition on very large data sets. *IEEE Trans. Pattern Anal. Mach. Intell.* **2005**, *27*, 603–618. [CrossRef]